Empirical uncertainty bounds of damping estimates of an offshore wind turbine in idling conditions

Jonas Gad Kjeld[a,b,1,*], Luis David Avendaño-Valencia[a], Anders Brandt[c], Silas Sverre Christensen[a,d], Jacob Karottki Falk Andersen[b]

[a]*Department of Mechanical and Electrical Engineering, University of Southern Denmark, Campusvej 55, 5230 Odense M, Denmark*
[b]*Foundations, Vattenfall Vindkraft A/S, Jupitervej 6, 6000 Kolding, Denmark*
[c]*Department of Mechanical and Production Engineering, Aarhus University, Inge Lehmanns Gade 10, 8000 Aarhus C, Denmark*
[d]*Siemens Gamesa Renewable Energy, Borupvej 16, 7330 Brande, Denmark*

Abstract

Structural damping is a critical quantity for condition assessment and fatigue lifetime prediction in wind energy. Its estimation from operational vibration data comes with a considerable amount of uncertainty, derived from environmental and operational variability and from the quality of the estimation process itself. In this paper, we aim to determine experimentally the damping values and their least possible uncertainty bounds for the first two modes of an idling offshore wind turbine. For this purpose, we use field measurements from a 3.6 MW offshore wind turbine located at the DanTysk wind farm. We select a subset of cases from the wind turbine on idling condition for a confined interval of environmental and operational conditions, in an attempt to minimize operational variability in the damping estimates. In addition, we make a study on the adjustment parameters of the automated operational modal analysis method, aiming at obtaining most consistent damping estimates.

Keywords: Offshore wind turbines, vibration monitoring, damping estimation, automated operational modal analysis.

1. Introduction

One of the major costs of an offshore wind farm is related to the foundations that support the *Offshore Wind Turbines* (OWTs) themselves. The structural design of the foundation structure is mainly governed by fatigue loads, which in turn depend on the environmental and operational conditions in which the OWT operates. Fatigue loads on the foundations are normally assessed through numerical simulations where damping becomes a critical input parameter. Due to the complexity of the system and existing

*Corresponding author

Email addresses: jonas.kjeld@vattenfall.com (Jonas Gad Kjeld), ldav@sdu.dk (Luis David Avendaño-Valencia), abra@mpe.au.dk (Anders Brandt), ssv@sdu.dk (Silas Sverre Christensen), jacob1.andersen@vattenfall.com (Jacob Karottki Falk Andersen)

knowledge gaps, a number of simplifications and assumptions are introduced into these models [1]. Hence, the damping values applied in the simulations are affected by a certain level of conservatism. The actual damping of an OWT can only be estimated from measurements on the actual structure. Due to the physical size and variable operating conditions of OWTs, and the fact that it is impractical to excite the structure artificially, classical experimental modal analysis techniques are not suitable for accurate modal parameter identifications. Instead, *Operational Modal Analysis* (OMA) is preferred, as it only relies on measured response signals [1, 2, 3].

Estimation of modal parameters involves a certain degree of uncertainty. For OMA of large civil structures, it is known that in most cases *Modal Parameter Extraction* (MPE) methods yield consistent estimates of natural frequencies and mode shapes. Nonetheless, it is also known that corresponding damping values are more difficult to estimate reliably. Therefore, for OWT design, it is not only important to consider a point estimate of damping, but also to understand its variability –uncertainty bounds–.

From a theoretical perspective, the uncertainty of modal parameter estimates can be separated into bias or random errors [4, 5]. Bias errors originate from model misspecification, namely when the model behind the MPE method does not match the data. This happens either when the model order is too low or too high, or as non-linearity or non-stationarity in the data emerges. On the other hand, the random error (or variance of the estimates), arises from the underlying randomness either in the excitation or in the environmental/operational conditions. In overall, while it is possible to reduce both random and bias errors to a certain extent by controlling the experiment and adjusting the MPE method, there is an irreducible uncertainty that will always take part of the estimates.

Analytical methods can be used to quantify the uncertainty of modal parameter estimates based on the vibration data characteristics. This can be done by means of perturbation methods attempting at determining the sensitivity of modal parameters to variations in vibration response data [4, 5, 6]. More recently, Bayesian methods have been introduced, which attempt at obtaining a probability density function of the modal parameters conditioned on the observed data [7, 8]. These uncertainty quantification methods have been mostly validated on numerical or controlled short-term monitoring data, and have demonstrated a good match between analytical and experimental results.

Nonetheless, uncertainty in modal parameter estimates explodes when performing OMA on long-term monitoring data, especially in the case of OWTs. Main factors comprise [9, 10]:

- The significant variability of environmental conditions, which introduces slowly-changing non-stationary dynamics. For instance wind and wave properties, precipitations, soil conditions and temperature.
- The associated changes on operational regimes (standstill, idling, normal power production, and so on) following wind conditions and operational demands, which shift the OWT dynamics between different regimes.

Variable operational regimes lead to different types of dynamics when the OWT is at standstill, idling or producing power. In particular, if the blades are rotating, time-periodic dynamics are activated, which violates the assumption of linear time invariant dynamics considered in most OMA methods. In practice, this means that damping estimates are less precise unless the OMA method directly addresses time-periodic dynamics [11, 12]. Otherwise, to avoid the effect of rotational dynamics, most studies are limited to standstill or idling conditions of the wind turbine [2, 3, 13].

Moreover, even if the OWT is at standstill or parked, its dynamics are sensitive to environmental and operational factors. Thus, damping estimates obtained from any MPE method will be comprised by different contributions derived from structural, aeroelastic and hydroelastic dynamics, and other factors including soil and tuned mass-damper contributions [3, 14, 15]. Consequently, it is necessary to decouple all these contributions before being able to assess any of the contributing factors. To do so, it is necessary to (i) shrink the analysis period to limit the effect of non-stationarity in the MPE method, but still long enough to facilitate consistent estimates; and (ii) correlate damping estimates with environmental factors so that their effect can be isolated, or minimize the variability of environmental factors in the dataset, so that uncertainty of modal parameter estimates is minimal [14, 16]. The first condition sets a tradeoff for the optimal analysis period; the second implies measurement of additional environmental parameters or a limitation of the cases included in the analysis.

Other factors include the effect of the MPE method itself. Some studies have made a comparison of the performance of various MPE methods [1, 15, 16, 17], concluding that while in overall most methods are able to detect the resonances, the lowest uncertainty is achieved with methods related to the *Covariance-driven Stochastic Subspace Identification* (SSI-COV) algorithm, which includes also the *Multi-reference Ibrahim Time Domain* (MITD) method [18]. Nonetheless, the optimal performance of each algorithm is bound to various decisions, for instance the data length, the number of correlation lags, the model order, selected sensors, among others [17, 19, 20, 21].

Along these lines, there is also the problem of tracking and matching the modal parameter estimates obtained at different analysis periods. Due to the considered data volumes, the task of selecting physical modes from frequency stabilization diagrams needs to be automated in some way. This comprises some type of statistical analysis, like clustering [3, 2, 9], triangulation algorithms [22], or histogram bin analysis [23, 18]. As in the case of MPEs, the performance of these Automated OMA (AOMA) methods is determined by different selections made while tuning the algorithms. These selections are often made considering a particular structure of the correlation functions. However, these considerations can easily change due to the non-stationary nature of the vibration response of OWTs [18, 24, 25]. Therefore, it is not feasible to select a single set of adjustment parameters that will work optimally for an entire long-term monitoring session. So, even though there is a rough idea of the effect of these selections on the performance of AOMA methods, there is no precise knowledge of their actual significance. More precisely, how exactly these selections affect the estimates of damping from long-term monitoring data.

The **main aim of this work** is to determine experimentally the damping value and minimize the uncertainty bounds of the first two modes (fore-aft and side-to-side) of an idling OWT from long-term vibration monitoring data. In doing so, we make use of an AOMA method based on the MITD method on data from an idling OWT in a confined interval of environmental and operational conditions, and perform a study on various critical parameters (analysis period, correlation lags, model order, mode detection thresholds) influencing the estimates of damping, while attempting at coming as close as possible to the irreducible random error.

For this purpose, we use field measurements from a 3.6 MW offshore wind turbine (OWT) located at the DanTysk wind farm acquired in the period between June 2019 and June 2021. In a previous work [25], the uncertainty bounds for the total damping of an offshore wind turbine were investigated for a single one-hour idle case. In the present work, we extend the analysis to 71 idling cases selected from within this period, corresponding to a confined interval of environmental and operational conditions. This confined analysis is used to limit to a major extent the effect of environmental and operational variability in the uncertainty of damping estimates, so that the obtained uncertainty bounds are as close as possible to the irreducible error.

Accordingly, the **main contributions of this work** are: (*i*) the experimental determination of uncertainty bounds for damping of the first two OWT tower modes in the idling condition; (*ii*) the assessment of the influence of the different adjustment parameters of AOMA, including those of modal parameter estimation, required to obtain those minimal uncertainty bounds.

This work is organized as follows: in Section 2 we explain the experimental setup and main data sources used in this work; in Section 3 we discuss the main methodological procedures used for data analysis, including data preprocessing and automated operational modal analysis; in Section 4 we initially present a study on the effect of different adjustment parameters in the modal parameter estimates, and based on those findings, we provide the uncertainty bounds for damping estimates. Following this, we discuss our findings and compare them with other works in the literature in Section 5, while final conclusions of this work are presented in Section 6.

2. Experimental setup

The field measurements investigated in this paper originate from a 3.6 MW Siemens offshore wind turbine located at the DanTysk windfarm in the North Sea. The turbine is 95 meters tall with a rotor diameter of 120 meters equipped with 9 high-accuracy triaxial DC accelerometers (model: *TRV-3301-1*) as shown in Figure 1. The height of all sensors is defined in relation to the Lowest Astronomical Tide (LAT) level. The accelerometers measure with a 1 % accuracy in the frequency range from DC to 100 Hz and the overall measurement accuracy for the calibration is 2.5%. Throughout this paper, sensors are enumerated top-down, so that the top sensor is named *Sensor 1*, while the bottom sensor is named *Sensor 9*. The accelerometers are connected to a *Data Acquisition* (DAQ) platform (Models: *IC-3171 Industrial Controller* and *NI 9239 BNC*). Vibration data is measured with a sampling frequency, f_s, of 25 Hz, with a measurement duration of one hour. A specifically developed system in LabView handles the storage of data records. From each triaxial accelerometer, only the two channels corresponding to the accelerations in the horizontal plane are considered in the subsequent analysis.

In addition to the dedicated tower acceleration measurements, operational and environmental data sampled with 10 Hz is also available from the Siemens *Turbine Condition Monitoring* (TCM) system installed at the nacelle. Information includes rotor speed, yaw angle, pitch blade angle, wind speed, and acceleration measured in both the fore-aft and the side-side direction at the nacelle. Additional environmental data, comprising wave height (sampling period of 60 seconds), and wind and wave direction (sampling period of 600 and 1800 seconds, respectively) are collected from the Research platform in the

North Sea and Baltic Sea No. 3 (FINO3), which is a meteorological mast located less than 3 km from the turbine investigated in this paper.

The main properties of the three data sources considered in this work are summarized in Table 1. As these data sources originate from independent measurement systems, direct synchronization could not be enforced. We show how the synchronization issue was solved in Section 3.

Table 1: Main properties of the three data sources used in this work

Data source	**Data streams**	**Sampling rate**
Dedicated tower monitoring system	Horizontal accelerations at 9 levels in the tower	25 Hz
Siemens TCM system	Rotor speed, yaw angle, pitch blade angle and wind speed	10 Hz
	Nacelle acceleration (fore-aft and side-to-side)	10 Hz
FINO3 meteorological mast	Wind direction, wave direction and wave height	1/600, 1/1800 and 1/60 Hz, respectively

3. Methodology

3.1. Preprocessing of experimental data

Synchronization of data streams. Since the tower acceleration signals and yaw angle originate from independent measurement systems, it is necessary to synchronize first the two systems and adjust the timestamps accordingly. For this purpose, we assess the cross-correlation between the tower acceleration data with the nacelle acceleration data from the TCM system (synchronized with the yaw angle) and determine the time lags required to achieve maximum correlation. Cross-correlation is measured in terms of the *Time Response Assurance Criterion* (TRAC) calculated between the two vectors formed by the acceleration time series of each of the analyzed signals [26]. The TRAC is defined as follows:

$$\mathrm{TRAC}_{xy} = \frac{\left[\{x\}^T\{y\}\right]^2}{[\{x\}^T\{x\})(\{y\}^T\{y\}]} \tag{1}$$

Rotor orientation alignment. Accurate identification of the fore-aft and side-side modes in subsequent OMA requires a precise value of the *Rotor Nacelle Assembly* (RNA) orientation with respect to each sensor location. This can be done with the use of the expression:

$$\begin{bmatrix} z_{fa}(nT_s) \\ z_{ss}(nT_s) \end{bmatrix} = \begin{bmatrix} \cos\Psi & \sin\Psi \\ -\sin\Psi & \cos\Psi \end{bmatrix} \begin{bmatrix} z_{X+}(nT_s) \\ z_{Y+}(nT_s) \end{bmatrix} \tag{2}$$

where $z_{X+}(nT_s)$ and $z_{Y+}(nT_s)$ indicate the original measured time series in the X and Y directions, and $z_{fa}(nT_s)$ and $z_{ss}(nT_s)$ indicate the transformed fore-aft and side-to-side time series.

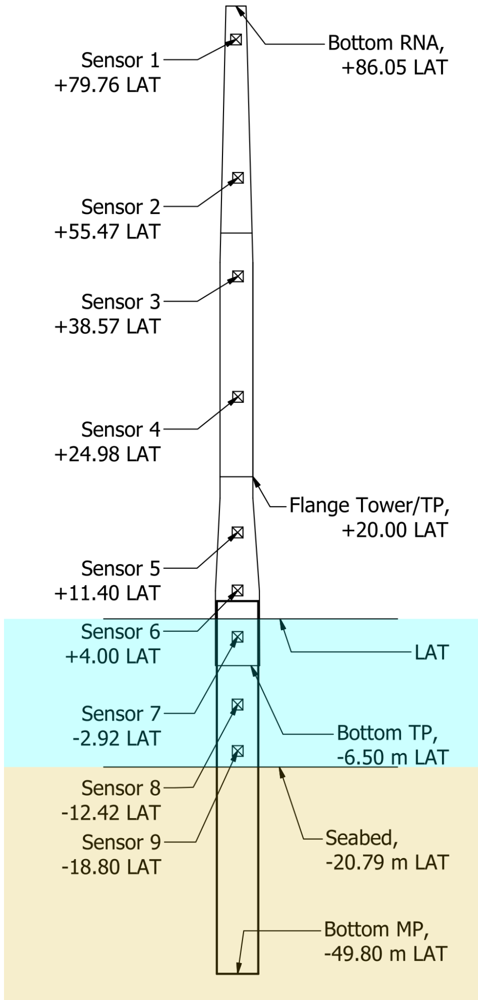

Figure 1: The nine accelerometer locations inside the wind turbine under analysis, measured from the seabed. LAT: Lowest Astronomical Tide (level); TP: Transition Piece; MP: MonoPile; RNA: Rotor Nacelle Assembly.

Once synchronization is in place, the RNA orientation can be derived from the yaw angle plus a small offset in the orientation of individual sensors. This offset can be calculated again by comparison between the highest tower accelerometer (Sensor 1) and the nacelle acceleration signal. Thus, we calculate the TRAC between these two signals while looking for the rotation that maximizes the obtained TRAC. The corresponding angle of rotation for this transformation is subtracted from the yaw angle to find the misalignment between Sensor 1 and the TCM accelerometer. This misalignment was found to be 0.6 degrees and the sensor orientations are adjusted accordingly prior to the transformation of coordinate systems. For subsequent analyses, the local sensor frame of reference is transformed into the the nacelle coordinate system to achieve a direct identification of the fore-aft and side-side modes.

Filtering of idling cases. For estimation of uncertainty bounds from AOMA, we want to limit to the maximum the uncertainty due to operational and environmental variability, so that cases with similar modal properties are considered in the analysis. To this end, we consider responses only from the *idling case*. Presently, the idling condition is defined as the operational condition when the offshore wind turbine produces no power (very low rotor speed) but is not at standstill (rotor is locked) and the blades are feathered (blades of the turbine are pitched parallel to the airflow). The latter makes the aerodynamic damping contribution from the rotating blades almost negligible (for increasing rotor speeds, the aerodynamic damping contribution overshadows the remaining damping contributors including hydrodynamic damping, structural damping, soil damping, and the built-in slosh damper). The idle and standstill conditions are separated as these have different dynamic characteristics. Standstill occurs only during maintenance under mild environmental conditions whereas idling cases are mostly related to scenarios where the turbines are supposed to not produce any energy. In the latter, the environmental conditions can be much more extreme in comparison to the standstill. For this reason idle cases are often more important to investigate from a design point of view. The logical criteria for defining the idle condition are summarized in Table 2.

Table 2: Definition of the idle condition

Cond. 1	Minimum pitch angle $\geq$ 80 degrees*
Cond. 2	Maximum rotor speed $\leq$ 1.5 RPM
Cond. 3	Minimum rotor speed $\geq$ 0.005 RPM
Cond. 4	Maximum variation in yaw angle $\leq$ 15 degrees

* *Rotor blades are feathered in an 82.5-degree pitch angle.*

In addition to these criteria, data are also clustered in terms of a confined interval of environmental and operational parameters. The intervals used to define the cluster of data used for subsequent analysis are shown in Table 3. With more than two years of measured acceleration data, these criteria leave us with a total of 70 data sets, each containing one-hour measurements for a particular cluster.

Table 3: Intervals for environmental and operational parameters

Parameter	**Notation**	**Unit**	**Min. value**	**Max. value**	**Mean value**
Wind speed	U	[m/s]	2.7	4.9	3.7
Wave height	H_s	[m]	0.6	0.9	0.7
Yaw misalignment	θ_y	[deg]	0.0	9.6	4.1
Wave misalignment	θ_w	[deg]	0.6	173.1	58.4

Further data quality checks. Finally, a number of statistical checks are carried out in order to avoid systematic errors in time data caused by measurement inaccuracy. These checks include kurtosis, skewness, and RMS. If any of these measures show erratic values for a given time data block, then it will not be processed any further. The original time signals are also de-trended by applying a high-pass Butterworth filter (filter order: 6, cutoff frequency: 0.1 Hz).

Regarding wave misalignment, the wave direction does not necessarily follow the nacelle orientation for the idle cases investigated. Wave height is relatively low (less than one meter) across the data sets. Therefore, it is assumed that the misalignment has a negligible influence on the modal properties of the system. It must be noted that the wind direction used to calculate the yaw misalignment originates from the FINO3 database and should not be confused with yaw error. The wind direction measured at the turbine itself was not available for this paper and there might be a small variation compared to the wind directions measured at FINO3.

3.2. Automated Operational Modal Analysis – Obtaining stable damping estimates

3.2.1. Modal Parameter Extraction

Modal parameters are estimated using the *Multi-reference Ibrahim Time-Domain* (MITD) method [27], which is an extension of the Ibrahim time domain method presented in [28] and bears several similarities with the *Stochastic Subspace Identification* (SSI) method [29]. MITD allows for multiple references to be included and is applicable for OMA since it works on free decay (correlation function) estimates. Thus, the first step in the MITD method comprises building the so-called Hankel matrix based on correlation functions. The size of the Hankel matrix depends on the number of lines (correlation lags) included from the correlation functions and the number of references. Subsequently, the second step involves the compression of the Hankel matrix with the help of the *Singular Value Decomposition* (SVD). Since the correlation function of the noise (typically broadband noise) dies out fast, the first few time lag values are usually skipped. According to [19], the first 4-8 time lag values should be disregarded to avoid measurement noise.

For autocorrelation and cross-correlation estimates of time signals, an unbiased and consistent estimator is sought. This is achieved by deriving cross-correlation estimates from cross-spectral power spectral density estimates using Welch's method. The cross-correlation estimator is compensated by the reciprocal of the Bartlett windows as described in [30]:

$$\hat{R}_{yx}(m) = \begin{cases} \frac{N-r}{N\Delta t}\hat{R}_{yx}(r), & \text{for } r = 0, 1, ..., N-1 \\ \frac{r-N}{N\Delta t}\hat{R}_{yx}(r), & \text{for } r = N, N+1, ..., 2N-1 \end{cases} \tag{3}$$

where $\hat{R}_{yx}(r)$ is the cross-correlation estimate calculated as the inverse DFT of the cross-spectral density estimate using Welch's method, N is the block size, and Δt is the time increment.

The MITD method, as for most modal parameter extraction methods, requires determination of the optimal range of model orders which yields better modal results. This is often assessed through stabilization diagrams in which a graphical representation of the estimated natural frequencies is displayed for increasing model orders. Poles that are unaffected in terms of frequency by changing model order are identified as probable physical modes, while those affected by changing model order are referred to as computational or spurious modes. Identification of the probable physical modes of the system from stabilization diagrams requires certain user expertise and becomes a tedious process when multiple data sets are involved. Here we consider an automatic modal parameter extraction procedure, as described next.

3.2.2. Automated Operational Modal Analysis

In this section, we describe an *Automated Operational Modal Analysis* (AOMA) algorithm based on the procedure initially presented in [23]. The AOMA algorithm is based on estimates of the poles and the respective mode shape vectors (or modal participation factor) obtained using any MPE method –here MITD–. The procedure can be summarized in the following steps:

1. **Histogram of natural frequencies:** A statistical representation of the pole estimates for different model orders is obtained by fitting a histogram to the natural frequency estimates.
2. **MAC calculation:** The *Modal Assurance Criterion* (MAC) is calculated between all mode shape vectors for every bin in the histogram whose frequency of occurrence is above a certain threshold. For completeness, the definition of the MAC is provided below, as follows [30, 31]:

$$\mathrm{MAC}_{rs} = \frac{|\{\Psi\}_r^H \{\Psi\}_s|^2}{(\{\Psi\}_r^H \{\Psi\}_r)(\{\Psi\}_s^H \{\Psi\}_s)} \tag{4}$$

   where $\{\Psi\}_r$ and $\{\Psi\}_s$ represent the mode shapes under study, and ^{H} denotes the Hermitian transpose (conjugate transpose) of the mode shape vector.
3. **Merging of histogram bins:** Poles from neighboring bins of the histogram are merged if their MAC value satisfies the specified MAC threshold criteria. This is more computationally intensive than the AOMA procedure where neighboring modes in terms of frequency are compared to the mean mode shape vector of a particular bin.
4. **Summary statistics of physical modes:** Mean and standard deviations of the pole and mode shape vector estimates are calculated for each probable physical mode.

In our implementation of the AOMA algorithm, the following adjustments are used:

1. **Bin width:** As the present analysis focuses only on the first two tower natural frequencies, falling in the range $[0.28, 0.34]$ Hz, the bin width is adjusted so a sufficient number of bins are set in the frequency range of interest. Accordingly, a bin width of $0.3\ Hz/300 = 0.001\ Hz$ is selected, which gives a maximum of 60 bins within the frequency range.
2. **Occurrence threshold:** The minimum number of stable estimates required in each bin of the histogram to be considered a probable physical mode is set to 15 % of the maximum model order.
3. **Identification of physical modes based on the MAC:** For each histogram bin, a respective MAC matrix is calculated for all the poles in the bin. A *master* mode is first selected as that corresponding to the row of the MAC matrix with most poles higher than a user-specified threshold (MAC_1). Subsequently, all the remaining modes associated with the master mode are selected by comparing with a secondary user-specified threshold (MAC_2). All the modes selected with the latter threshold are considered to belong to the same mode.

The estimated mode shapes from the MITD method come with an arbitrary scaled phase - the imaginary part of the mode shape vector. In the AOMA, mode shapes are normalized according to the maximum of the absolute value of the imaginary parts. This results in a maximum real part of 1 and a minimum imaginary part of 0. The normalization does not influence the modal parameters but affects the MAC calculation between mode shapes obtained from different data sets slightly (on 3rd decimal place). The reason why the normalization influences the MAC calculation very little is that the imaginary part of the mode shapes is almost negligible.

3.2.3. Application in the dataset of idle cases

The following procedure has been carried out to identify the fore-aft and side-side modes on the 70 idle cases:

1. **Study of input parameters for modal parameter extraction**: AOMA is carried out on each of the 70 data sets by applying the MITD method with changing input parameters including measurement duration, reference combination, and number of lines included from the correlation functions.
   (a) Probable physical modes are identified within the interval [0.28, 0.34] Hz and a minimum MAC value of 0.94 between all modes for a particular frequency bin in the histogram.
   (b) A *reference mode shape vector*[1] is established for the fore-aft and side-side modes, respectively, as shown in Figure 2 and evaluated at the sensor locations from Figure 1 included in the analysis. For each analysis, the MAC is calculated between identified modes in the AOMA and the two reference modes separately. If a MAC value is larger than 0.8, the particular mode is identified as either fore-aft or side-side depending on the reference mode.
2. **Collecting identified modes from every data set**: All identified probable physical modes, n_p, for an optimal set of input parameters including all 70 data sets are collected, that is:

$$n_p = \sum_{n=1}^{N} \sum_{m=1}^{M_n} K_{nm}$$

   where N is the number of data sets ranging from 1 to 70, M_n is the number of bins that contain probable physical modes for each data set n, and K_{nm} is the number of probable physical modes contained in each bin ranging from 15 to 100.
   (a) The MAC is calculated on all mode shape vectors and a *master mode* for each of the fore-aft and side-side mode is identified. The *master mode* is the mode that has the most mode shape vectors in common for a MAC threshold greater or equal to 0.95.

[1]The reference mode shape vector is based on a finite element (FE) model which is built on the same geometry and soil conditions of the OWT that is investigated in this paper. The FE model is two-dimensional and uses the mass moment of inertia of the RNA in the fore-aft direction. The mode shape vector of the first bending mode (corresponding to the fore-aft mode) is assumed to be very similar to the side-side mode and will create the basis for both reference modes (orthogonal to each other).

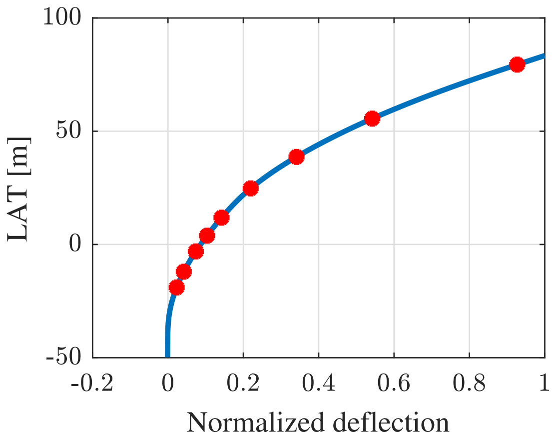

Figure 2: Reference mode obtained from an FE model based on the OWT investigated in this paper. (—) refers to the mode shape vector defined in all DOFs (135) of the FE model and ● is the mode shape vector of the FE model evaluated at *Sensor 1* to *Sensor 9*, with 1 having the highest deflection and 9 the lowest.

4. Results

4.1. Study of input parameters for modal parameter estimation

This section provides an analysis of the adjustment parameters used as input to the MITD method, with the aim of assessing their effect on the modal parameter extraction results and determining optimal (or close to optimal) selections. The analysis presented below comprises variations of:

1. Measurement duration (number of 10-minute time-blocks combined)
2. Combination of sensors (references)
3. Model order and number of lines included from correlation functions

Table 4 lists the fixed input parameters applied to all data sets in the AOMA based on the MITD method. $\mathrm{N}_{\mathrm{lines}}$ indicates the number of lines used from the correlation function, $\mathrm{M}_{\mathrm{order}}$ the model order, and the two MAC tolerances (MAC_1 and MAC_2) refer to the adjustments made to the AOMA algorithm described in 3.2. For each histogram bin, the MAC_1 tolerance of 0.98 finds the *master mode* which has the most modes in common in terms of mode shape vectors. The MAC_2 tolerance of 0.94 sets the lower threshold for what we allow the minimum MAC value to be among the cluster of poles found by the first MAC tolerance. The frequency tolerance refers to the histogram bin width which groups the pole estimates from the stabilization diagram. Bin width is set to 0.25 % of the first natural frequency of approximately 0.3 Hz, which was found to give good results in preliminary runs. Neighboring poles in terms of frequencies are also investigated only if they lie within $\pm 2\times$ *bin width* thus resulting in a maximum variation in frequency, f_{tol}, of $0.3\,\mathrm{Hz}/100 = 0.003\,\mathrm{Hz}$.

Effect of measurement duration. Figure 3 shows the mean and *Coefficient of Variation* (CoV) of the damping ratio estimates –color hue– and the number of successfully identified modes –numbers by data points– obtained from 42 idle cases with measurement

Table 4: Input for automated modal parameter estimation

$\mathbf{N_{lines}}$	$\mathbf{M_{order}}$	$\mathbf{MAC_1}$	$\mathbf{MAC_2}$	$\mathbf{f_{tol}}$	**References**	**MPE method**	**Normalization method**	$\mathbf{f_s}$	**T**
[-]	[-]	[-]	[-]	[Hz]	[-]	[-]	[-]	[Hz]	[s]
[10:110]	[1:100]	0.98	0.94	0.3 Hz/100	Sensor 1, 2, 3 and 4	MITD	High	25	3600

duration ranging from 10-minutes to 120 minutes. The number of cases is reduced to 42 in this study, as the measurement duration is extended to 120 minutes. AOMA is capable of identifying two modes with distinct damping ratios (fore-aft and side-side modes) for any measurement duration ranging from 10 to 120-minutes. The mean and CoV of damping ratios stabilize after 50 minutes for the fore-aft modes, and after 60 minutes for the side-side mode. The decision on the measurement duration comprises a trade-off between including as many blocks of data as possible and maximizing the number of cases that fulfill the idling criteria. For the particular cluster of data investigated in this work, the resulting number of cases that fulfill the idle criteria is highly affected by the measurement duration (70 one-hour idle cases versus 42 two-hour idle cases). By choosing a measurement duration of 60 minutes, the damping is nearly unaffected by increasing measurement duration and the CoV of damping ratios is at 0.11-0.15 % for both identified modes (0.13-0.18 % for 50-minutes measurement duration).

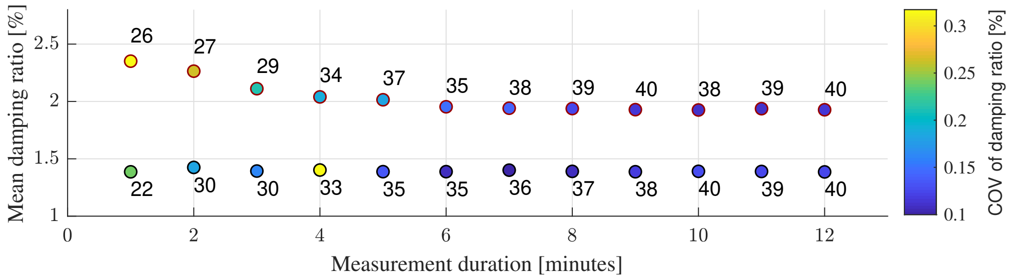

Figure 3: Mean and CoV of damping ratios of 42 idle cases as a result of changing measurement duration (number of combined 10-minute time-blocks). refers to fore-aft modes and refers to side-side modes. Numbers next to each circle indicate the number of successful identifications.

Sensor combinations. The influence of different sensor combinations in the MPE calculations was also investigated for all 70 idle cases. However, for brevity, we report only the main results. Mean damping ratios in the fore-aft direction are relatively consistent for any reference combination as long as at least one sensor located higher than *Sensor 5* is chosen. The sensor combination *Sensor 1, 2, 3* and *4* appear to be sufficient to achieve consistent damping estimates in terms of mean values and CoV and will be applied in the later analysis of this paper.

Model order and number of correlation lines. The number of lines included from the correlation functions that give the most consistent modal parameters is more difficult to assess. One of the success criteria for good modal parameter estimation is the quality of the stabilization diagrams. This is usually determined by the presence of a large number of pole estimates which are unaffected by changing model orders. In Figure 4a and Figure 4b, the number of stable estimates for all 70 data sets are shown for different numbers of lines and model orders. It is observed that AOMA finds the most stable poles when using few lines from the correlation functions and for model orders higher than 20. When 110 lines are included from the correlation functions, 48 or more data sets are identified, as observed in Figure 4a and 4b. Still, while having a high number of stable estimates measures the quality of the stabilization diagram, it is not a guarantee for a high quality of the obtained modal parameter estimates, since there may still be bias errors in the estimates.

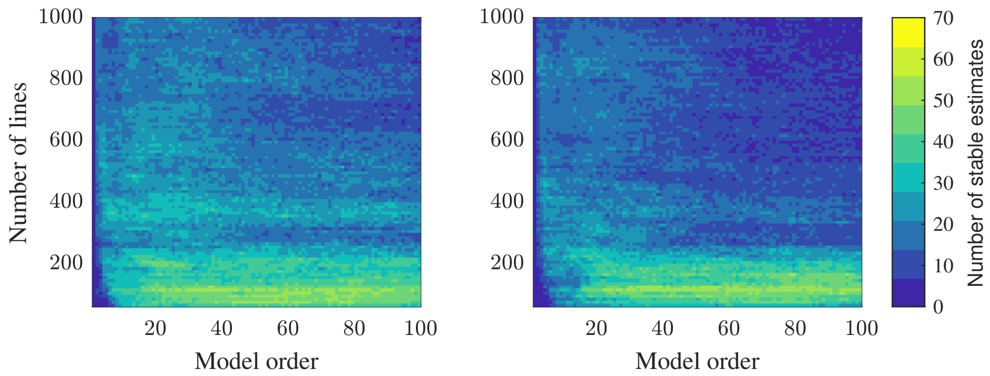

(a) Fore-aft mode

(b) Side-side mode

Figure 4: Number of stable estimates for all 70 data sets for every model order and including from 60 to 1000 lines (step size 10) from the correlation functions.

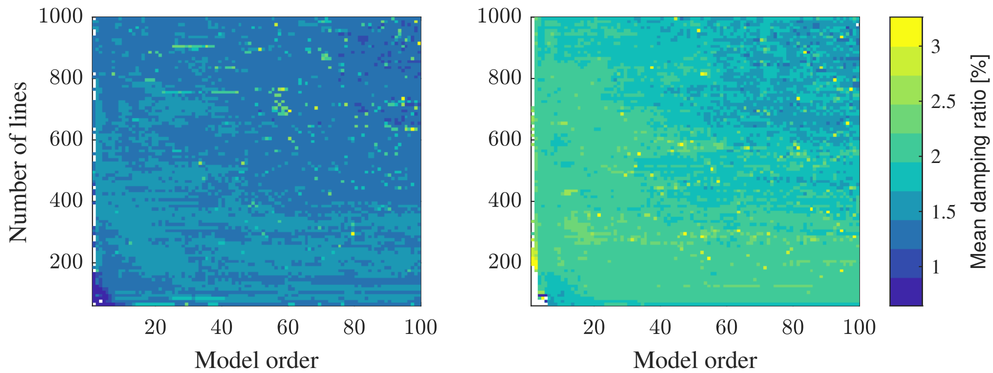

(a) Fore-aft mode

(b) Side-side mode

Figure 5: Mean damping ratio for all 70 data sets at every model order and with 60 to 1000 lines (step size 10) included from the correlation functions.

The quality of the estimates can be assessed through the results in Figures 5 and 6, illustrating the mean damping ratio and CoV for each mode. In this case, the mean damping ratio seems to be more consistent between 60 and 300 lines across model orders ranging from almost 20 to 100 for both identified modes. The CoV of damping ratios

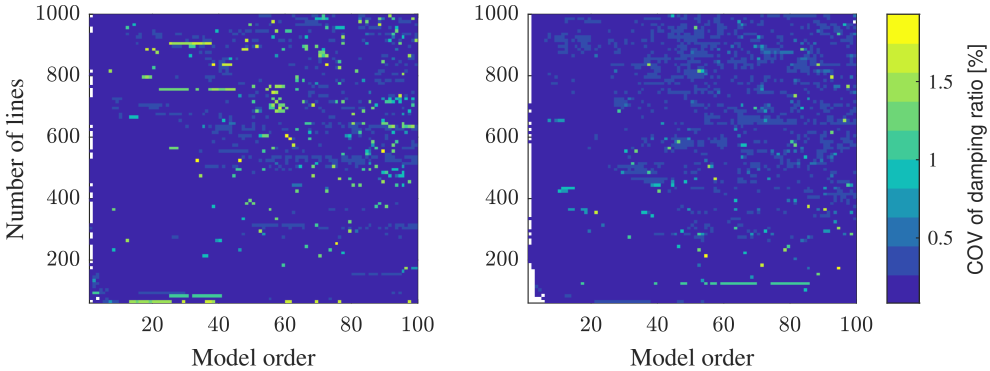

(a) Fore-aft mode

(b) Side-side mode

Figure 6: Coefficient of Variation of damping ratio for all 70 data sets at every model order and number of lines included from the correlation functions ranging from 60 to 1000 with a step size of 10.

appears to be more dispersed overall. However, for numbers of lines ranging from 110 and 150, the CoV is near 0 and quite consistent across all model orders.

As a result, for later analyses, 110 lines will be included from the correlation functions for modal parameter extraction. This will facilitate:

1. A large number of stable estimates.
2. Consistent damping estimates across almost all model orders in terms of both the mean and the CoV of damping ratios.
3. Fore-aft modes for 55/70 data sets and side-side modes for 58/70 data sets which have a MAC value greater or equal to 0.8 to the reference mode shape.

Regarding the model order, Figure 4 shows that the largest number of stable estimates is found with a model order above 20 and Figure 5 shows a significant variation of damping ratios within the same region. Therefore, the first 15 model orders are ignored in the final analysis.

Our results can be contrasted with the recommendations presented in [19] related to the number of lines from correlation functions to be used for modal parameter extraction. It was shown that for multiple DOF systems, the random error of the correlation function estimates increases for increasing number of lines. This can explain why more consistent modal parameters are obtained when few lines are extracted from the correlation functions. Simultaneously, the random error decreases with a higher available measurement duration as a consequence of fewer overlapping samples in the correlation function estimates. It was also shown that the damping ratio was highly sensitive to the measurement duration and damping values were overestimated if the duration was too short, which is consistent with the findings presented here.

4.2. Detailed analysis of the influence of the number of lines

By applying the input parameters from Table 4 into the MITD method, the AOMA is applied to identify and estimate modal parameters for all 70 idle cases. Figure 7 shows 4 examples of the auto-correlation functions of all included references (*Sensor 1-4*) for every degree of freedom. The auto-correlation functions for all cases show a well-defined and consistent free decay. In data sets 81643 and 82415, the correlation seems to die out after 1500 lines (corresponding to more than a minute with a sampling frequency of 25 Hz), while in datasets 84763 and 84886 the autocorrelation seems to remain much longer. This is an indication of the variable damping ratio.

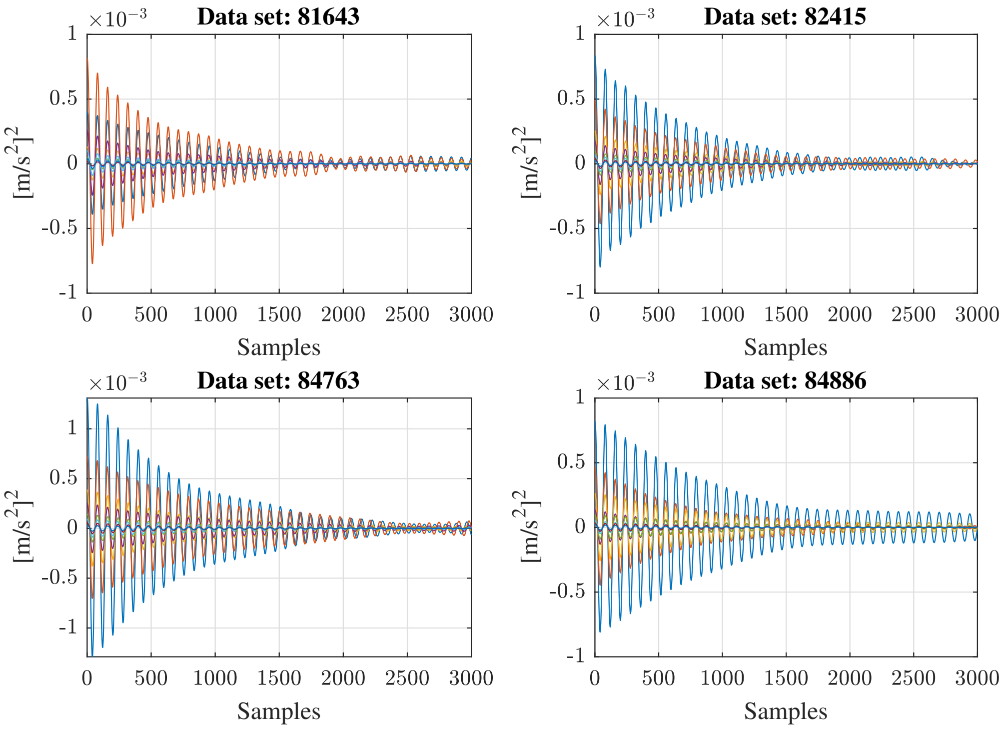

Figure 7: Sample auto-correlation function estimates for 4 different datasets. *Sensor 1, X+*: (——), *Sensor 1, Y+*: (——), *Sensor 2, X+,*: (——), *Sensor 2, Y+*: (——), *Sensor 3, X+*: (——), *Sensor 3, Y+*: (——), *Sensor 4, X+*: (——), *Sensor 4, Y+*: (——)

Continuing with the bottom two data sets *84763* and *84886*, the statistical representation of pole estimates based on 110 lines are shown in Figure 8. For every bin in the histogram, the stability of the poles is assessed by applying the MAC to the mode shape vectors. The resulting estimates are shown as stable (green asterisk) or unstable (red asterisk) in Figure 8. The green asterisks form patches that indicate the boundaries for a particular probable physical mode identified in the AOMA. For both cases, a large number of stable estimates can be seen for each of two modes that are well separated in terms of frequency.

For comparison, Figure 9 displays a similar statistical representation of pole estimates based on 700 lines for the same two data sets. In the case of dataset *84763*, both modes can be still identified, although these are less spaced in frequency. For data set *84886*, it is now not possible to discriminate between the two modes. This result originates from the larger influence of random error on the latter portion of the correlation functions.

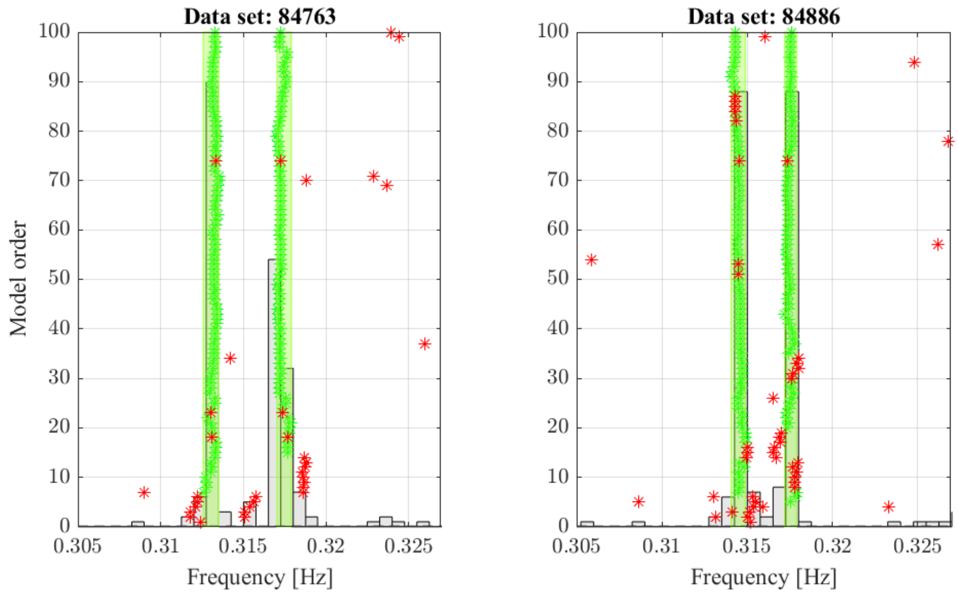

Figure 8: Histogram of pole estimates based on 110 lines. * refers to stable pole estimates and * refers to unstable pole estimates. indicates the boundaries of stable frequency estimates for each identified probable physical mode.

4.3. Collecting identified modes from every data set

As described at the beginning of Section 4, identical modes have been identified using a MAC threshold of 0.98 to identify the *master mode* and 0.94 as the minimum threshold for each analysis. When it comes to identifying similar modes across multiple data sets originating from different time points, a lower MAC tolerance is required to get any results, as the orientation of mode shape estimates from different datasets can be as high as 20 degrees. A MAC tolerance of 0.85 was applied between cases (as opposed to 0.98 applied in the individual case analysis) to find the *master mode*, and 0.72 is applied in order to ensure the minimum MAC value across all mode shapes that are similar to the *master mode*.

In Figures 10 and 11, results from all 70 data sets have been collected and the fore-aft and side-side mode have been identified by applying the 0.95 MAC threshold. The figures show the CoV of damping ratios for every model order ranging from 1 to 100 for both modes, separately. For the side-side mode, a significant change in the standard deviation of damping ratios for the first 12 model orders can clearly be seen. This is, however, less evident for the fore-aft mode, where the CoV seems to stabilize after the first 6 model orders.

Figures 12 to 14 show the results of a final AOMA carried out on all 70 idle cases by applying the *optimal* input parameters for the MITD method. These include a measurement duration of 1 hour, a reference combination of *Sensor 1, 2, 3*, and *4*, 110 lines included from the correlation functions, and model orders ranging from 16 to 100. Figure 12 shows the orientation of the mode shape vectors evaluated at *Sensor 1*. The maximum

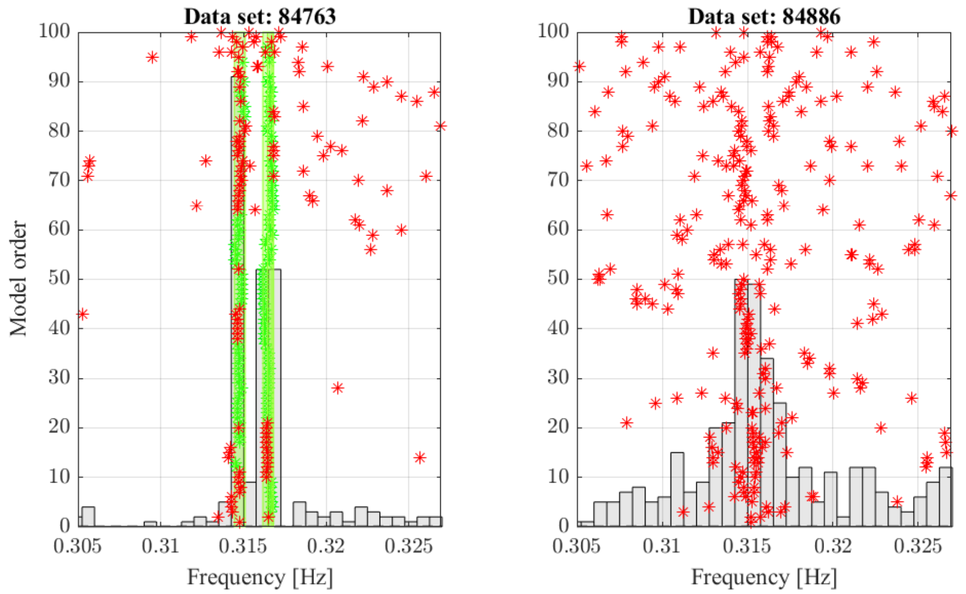

Figure 9: Histogram of pole estimates based on 700 lines. * refers to stable pole estimates and * refers to unstable pole estimates. indicates the boundaries of stable frequency estimates for each identified probable physical mode.

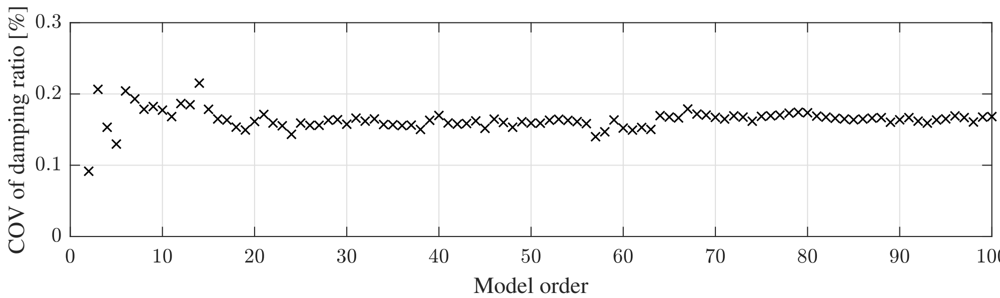

Figure 10: Standard deviation of damping estimates for each model order - Fore-aft mode

variation in orientation for a single data set is 13 degrees for the fore-aft mode and 10 degrees for the side-side mode. Across all represented data sets, the maximum variation in orientation for the fore-aft mode is 25 degrees and 26 degrees for the side-side mode. This variation is limited by the MAC threshold of 0.94 applied to identify probable physical modes. In 20 cases, the fore-aft and side-side modes were identified simultaneously. The mean difference in orientation between the two modes for these 20 cases is 94 degrees with a CoV of 0.09.

The damping ratio for the fore-aft and side-side modes at different model orders ranging from 16 to 100 is shown in Figures 13a and 13b, respectively. There are no clear outliers for any of the two modes. However, a small cluster of datapoints is observed

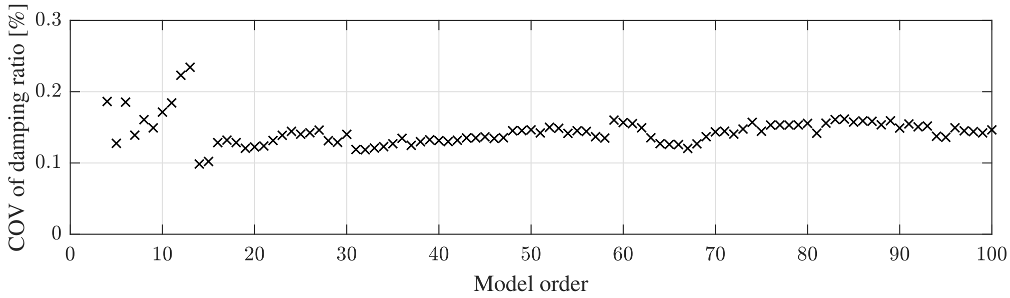

Figure 11: Standard deviation of damping estimates for each model order - Side-side mode

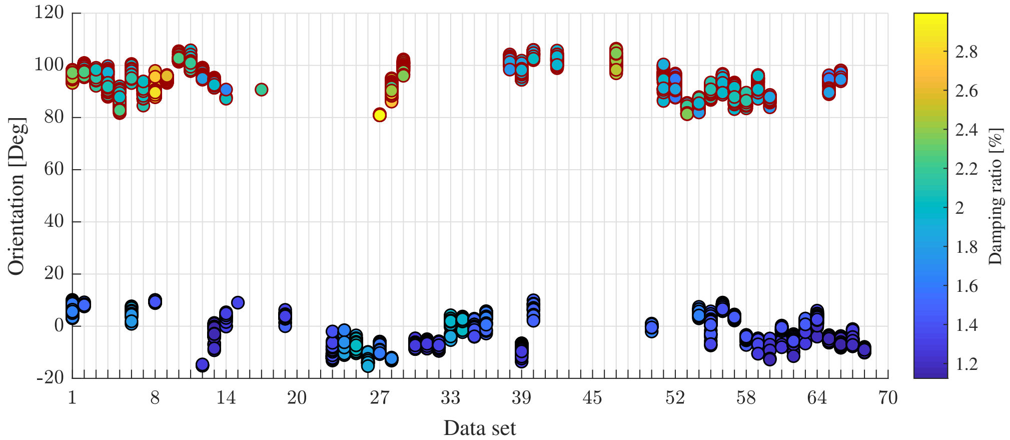

Figure 12: Orientation of mode shapes at *Sensor 1* for all model orders in the range of 16 to 100 from all data sets. ○ (orientations around 0) refers to fore-aft modes and ○ (orientations around 90) refers to side-side modes

towards higher damping values in both cases, which is slightly separated from the remaining estimates. This is more evident for the fore-aft mode in comparison to the side-side mode.

In Figure 14a is displayed a scatter plot with natural frequency and damping estimates for both fore-aft and side-to-side modes. After considering the MAC threshold of 0.95 to find the *master mode* for each of the two modes, two clusters of data points are clearly visible (× and ×). In comparison to all results (transparent gray circles) identified by the reference mode shape, data points contained in the two clusters are well separated both in terms of frequencies and damping ratios. It should be noted the maximum variation in natural frequencies of the two clusters is 1.3 % and 1.1 % for the fore-aft and the side-to-side mode, respectively. In Figure 14b is illustrated the histogram for the damping estimates of each one of the modes across all datasets. The distribution of damping ratios for each of the two identified modes is quite similar. For both cases, two bins are very dominant with more than 500 estimates whereas most of the remaining bins contain less than 200 estimates.

Table 5 provides a summary of the results from Figures 13a and 13b. The 90 %

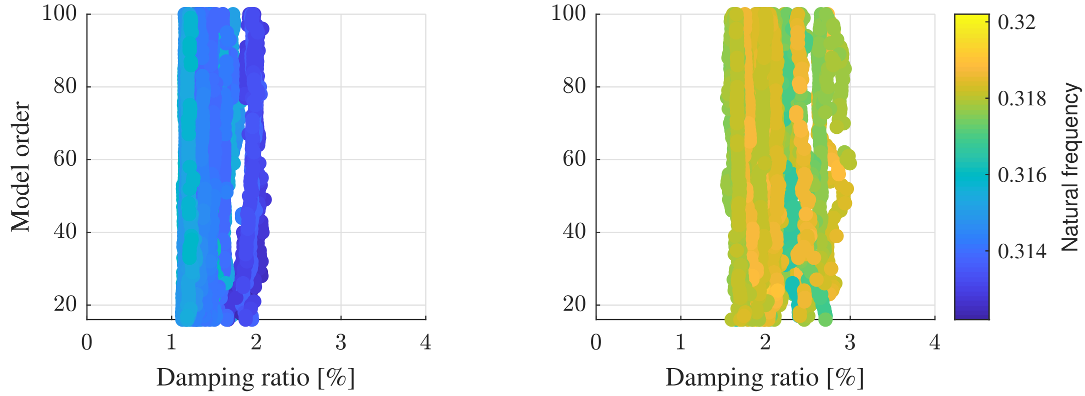

(a) Damping estimates vs model order - fore-aft mode

(b) Damping estimates vs model order - side-side mode.

Figure 13: Damping ratios for model orders ranging from 16 to 100 for all data sets calculated from 110 lines

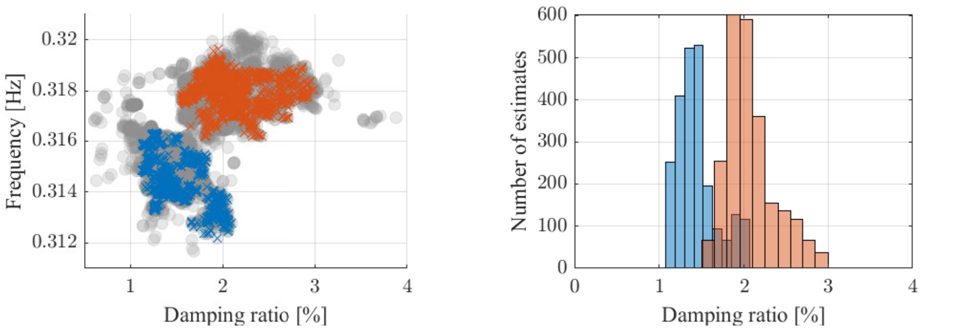

(a) Frequency vs damping ratio. × refers to the fore-aft mode and × refers to the side-side mode. Transparent gray circles refers to all results prior to collection of identified modes.

(b) Histograms of damping estimates. refers to the fore-aft mode and refers to the side-side mode.

Figure 14: Frequency and damping estimates for all data sets using an *optimal* set of input parameters for the MITD method.

confidence interval captures the damping ratios from the fore-aft mode between 1.2 and 2.0 % damping. For the side-side mode, the range is from 1.7 to 2.7 % damping. The increased range in damping for the side-side mode in comparison to the fore-aft is most likely because the aerodynamic damping is larger in comparison to the fore-aft mode. Wave frequency was not included in the 70 idle cases but it was shown to have almost no influence on the modal parameters or the 90 % confidence interval for these cases presented in Table 5. The environmental and operational parameter intervals as a result of collecting identified modes obtained from the AOMA are listed in Table 6. The ranges are slightly different from the ones listed in Table 3. The upper boundary of the wind speeds (4.9 m/s) is reduced to a maximum of 4.4 m/s and the upper boundary of the yaw misalignment (9.6 degrees) is reduced to 6.4 degrees. The maximum value for the wave misalignment has also been reduced significantly where cases with wave directions almost 180 degrees to the yaw direction are left out. Within the intervals listed in Table 6, there is no noteworthy correlation between the different parameters and damping ratio. Information such as the temperature and scour depth was not available for this paper and these may very well influence the damping ratio.

5. Discussion

For both modes shown in Figure 14b, there are a significant number of larger damping ratios compared to the bins which contain the most estimates. For the side-side mode, these larger damping estimates most likely originate from aerodynamic damping caused by the feathered blades of the rotors and wave loading acting upon the structure from different directions. As explained in [32], the aerodynamic forces are present for the side-side mode during idle conditions. The feathered blades create a larger surface in the transverse direction of the nacelle orientation (side-side) that interacts with the surrounding air. In [2], it was shown that higher drag forces in case of higher wind speeds result in higher damping estimates for both the fore-aft and the side-side mode.

Any of these two explanations for an increment in damping caused by aerodynamic damping does not carry over to the fore-aft mode since the blade surface in this direction is very small and the wind speed only varies 1.4 m/s. The increase in damping is most likely due to environmental and operational conditions that we do not account for. The variation in mode shape orientation shown in Figure 12 also indicates that there are some discrepancies between measured directions of environmental and operational data. Another possible explanation is vortex-induced vibrations (VIV) - but the RMS value of measured accelerations during idle conditions does not show any significant increase at these wind speeds (4.1 m/s, Table 3), which it should if VIV was present.

The total number of estimates is very similar for the fore-aft and side-side modes of 2316 and 2387, respectively, as listed in Table 5. The success rate is slightly higher for the fore-aft modes in comparison to the side-side modes (73 % versus 60 %). The overall uncertainty in damping estimates for both modes is a result of random and bias errors occurring from the time series of the measured accelerations and the identification procedure.

As described in Section 2, the accelerometers measure with a ±1 % accuracy in the frequency range DC-100 Hz and a 2.5 % overall measurement accuracy for the calibration which introduces a bias error in the measurements. The bias error will not affect the pole estimation but could affect the mode shape estimation if two sensors have different sensitivity errors as mentioned in [19]. In addition to the sensitivity errors which may influence the mode shapes, large deflections of the tower structure caused by environmental and operational excitation influence the estimated mode shapes in all three directions. Since the measurement system is not connected to the vertical direction (z-direction) of the triaxial accelerometers, it has not been possible to investigate the influence of large deflections on the mode shape vectors. The vertical component for large deflections is considered to be negligible and therefore has no influence on the mode shape estimates. The uncertainty of the system identification process using the MITD method is much more difficult to assess because the true modal model is unknown. Only random errors affect the correlation functions since the calculation is based on the unbiased estimator. Since the measurement duration of each analysis is limited by the fact that we want stationary conditions in our time series, a random error is introduced caused by the truncation of our signal. Simultaneously, the random error increases the more information we include from the correlation functions thus limiting how many lines can be applied in the system identification. This is most likely the reason why damping is estimated more consistently by applying only 110 lines from the correlation functions compared to applying significantly more.

In [33], the soil damping was estimated to be 0.2 % for wind speeds of 5 m/s which is relatively close to the mean wind speed investigated in this paper (3.7 m/s) and up to 1.3 % for wind speeds of 12 m/s. Based on these findings, the increase in wind speeds within the range investigated in this paper (3 m/s to 4.4 m/s) may explain a few of the larger damping estimates present for both fore-aft and side-side modes. In [16], the average damping ratio was estimated between 2 % and 2.5 % for a similar offshore wind turbine across a larger span of wind speeds and wave heights. With the wind speeds and wave heights investigated in this paper, the damping ratio for the fore-aft mode found in [16] approaches 1.5 % whereas the damping ratio for the side-side mode is slightly higher. These values also fall within the 90 % confidence interval for each of the two modes listed in Table 5 ($\zeta_{5\%}$ and $\zeta_{95\%}$). In [2], the damping values for the first fore-aft and side-side mode and a wind speed of 4.5 m/s were found to be 1.2 % and 1.27 %, respectively, while the tuned mass damper (TMD) was deactivated. Both values are slightly lower than the 5 % fractile of 1.2 % and 1.7 % listed in Table 5 for the fore-aft and side-side mode, respectively, and this is most likely because the built-in slosh damper is activated for the results presented in this paper. It may also be affected by different soil conditions and structural differences. In [3], the mean damping ratios for the fore-aft and side-side mode are estimated at 1.73 % and 2.18 %, respectively, for wind speeds ranging between 4 m/s and 6 m/s with the TMD activated. With the TMD activated, the damping values for both modes are very close to the center of the 90 % confidence interval listed in Table 5.

Table 5: Results from collecting identified modes obtained from AOMA

Mode no.	**Description**	$\mathbf{f_{n5\%}}$	$\mathbf{f_{n95\%}}$	$\zeta_{5\%}$	$\zeta_{95\%}$	$\mathbf{N_{est}}$	**Success rate (Data set)**	$\mathbf{MAC_{min}}$
		[Hz]	[Hz]	[%]	[%]	[-]	[-]	[-]
1	Fore-aft	0.313	0.316	1.2	2.0	2316	40/55	0.81
2	Side-side	0.317	0.319	1.7	2.7	2387	35/58	0.81

Table 6: Environmental and operational parameter intervals as a result of collecting identified modes obtained from AOMA

Parameter	**Notation**	**Unit**	**Description**	**Min.**	**Max.**	**Mean**
Wind speed	U	[m/s]	Fore-aft	3.0	4.4	3.7
			Side-side	3.0	4.3	3.6
Wave height	H_s	[m]	Fore-aft	0.7	0.8	0.7
			Side-side	0.7	0.8	0.8
Yaw misalignment	θ_y	[Degree]	Fore-aft	0.3	6.4	2.7
			Side-side	0.3	6.4	3.2
Wave misaligntment	θ_w	[Degree]	Fore-aft	0.2	110.5	48.1
			Side-side	6.8	110.5	69.8

6. Conclusion

This paper presented the modal parameters of an offshore wind turbine during idling conditions achieved by using Automated Operational Modal Analysis (AOMA). The purpose of this paper was to investigate whether or not it is possible to estimate the damping ratio of the fore-aft and side-side mode of an offshore wind turbine with reasonable confidence by exploring the various input parameters applied in the modal parameter estimation method - in this case, the Multiple-reference Ibrahim Time Domain method. In the first step, acceleration measurements were synchronized with environmental and operational parameters obtained from different measurement systems. Secondly, comparable data sets labeled as *idle* were identified by taking multiple environmental and operational conditions into account including the yaw angle, blade pitch angle, rotor speed, wind direction, wind speed, and wave height. In the third step, modal parameters were estimated for each set of data using an AOMA. The final step was to combine modes obtained from idle cases identified as comparable and collect the results in a histogram to show the distribution of damping estimates.

It was possible to choose a set of values for input parameters for the modal parameter estimation which gave reasonably consistent modal parameter estimates. The significant input parameters included; a measurement duration of at least one hour, a reference combination of *Sensor 1, 2, 3* and *4*, model orders ranging from 16 to 100, and 110 number of lines included from the correlation functions. The 90 % confidence interval of the collected results was found to bound the damping within a range of 0.8 % and 1 % for the fore-aft and side-side mode, respectively. In [16], the average damping ratio was estimated between 2 % and 2.5 % for a similar offshore wind turbine across a larger span of wind speeds and wave heights. For wind speeds and wave heights comparable to the levels investigated in this paper, the damping ratios for the fore-aft and side-side mode fall within the 90 % confidence interval shown in Table 5.

Acknowledgments

We thank Morten Hartvig Hansen for his guidance and valuable discussions about the content of this paper. We also thank Jonas Vestermark for the many fruitful discussions that we had during the process of writing this paper.

The research presented in this paper is funded by Vattenfall Vindkraft A/S and the Innovation Fund Denmark.

Data was made available by the FINO (Forschungsplattformen in Nord- und Ostsee) initiative, which was funded by the German Federal Ministry of Economic Affairs and Energy (BMWi) on the basis of a decision by the German Bundestag, organized by the Projekttraeger Juelich (PTJ) and coordinated by the German Federal Maritime and Hydrographic Agency (BSH).

References

[1] **Makekjafarian, A., Jalilvand, S., Doherty, P.** and **Igoe, D.**, *Foundation damping for monopile supported offshore wind turbines: A review*, Marine Structures, Vol. 77, pp. 102937, 2021.

[2] **Devriendt, C., El-Kafafy, M., Sitter, G. D.** and **Weijtjens, W.**, *Monitoring resonant frequencies and damping values of an offshore wind turbine in parked conditions*, IET Renewable Power Generation, Vol. 8, No. 4, pp. 433–441, May 2014.

[3] **Shirzadeh, R., Weijtjens, W., Guillaume, P.** and **Devriendt, C.**, *The dynamics of an offshore wind turbine in parked conditions: a comparison between simulations and measurements*, Wind Energy, Vol. 18, No. 10, pp. 1685–1702, Jul. 2014.

[4] **Pintelton, R., Guillaume, P.** and **Schoukens, J.**, *Uncertainty calculation in (operational) modal analysis*, Mechanical Systems and Signal Processing, Vol. 21, pp. 2359–2373, 2007.

[5] **Reynders, E., Pintelton, R.** and **De Roeck, G.**, *Uncertainty bounds on modal parameters obtained from stochastic subspace identification*, Mechanical Systems and Signal Processing, Vol. 22, pp. 948–969, 2008.

[6] **Reynders, E., Maes, K., Lombaert, G.** and **Roeck, G. D.**, *Uncertainty quantification in operational modal analysis with stochastic subspace identification: Validation and applications*, Mechanical Systems and Signal Processing, Vol. 66-67, pp. 13–30, Jan. 2016.

[7] **Li, B., Der Kiureghian, A.** and **Au, S.-K.**, *A Gibbs sampling algorithm for structural modal identification under seismic excitation*, Earthquake Engineering & Structural Dynamics, Vol. 47, No. 14, pp. 2735–2755, 2018.

[8] **Sehedi, O., Katafygiotis, L. S.** and **Papadimitriou, C.**, *Hierarchical Bayesian operational modal analysis: theory and computations*, Mechanical Systems and Signal Processing, Vol. 140, pp. 106663, 2020.

[9] **Oliveira, G., Magalhães, F., Cunha, Á.** and **Caetano, E.**, *Continuous dynamic monitoring of an offshore wind turbine*, Engineering Structures, Vol. 164, pp. 22–39, 2018.

[10] **Avendaño-Valencia, L. D., Chatzi, E. N.** and **Tcherniak, D.**, *Gaussian process models for mitigation of operational variability in the structural health monitoring of wind turbines*, Mechanical Systems and Signal Processing, Vol. 142, pp. 106686, 2020.

[11] **Allen, M. S., Sracic, M. W., Chauhan, S.** and **Hansen, M. H.**, *Output-only modal analysis of linear time-periodic systems with application to wind turbine simulation data*, Mechanical Systems and Signal Processing, Vol. 25, pp. 1174–1191, 2011.

[12] **Chen, W., Jin, M., Huang, J., Chen, Y.** and **Song, H.**, *A method to distinguish harmonic frequencies and remove the harmonic effect in operational modal analysis of rotating structures*, Mechanical Systems and Signal Processing, Vol. 161, pp. 107928, 2021.

[13] **Carswell, W., Johansson, J., Løvholt, F., Arwade, S., Madshus, C., DeGroot, D.** and **Myers, A.**, *Foundation damping and the dynamics of offshore wind turbine monopiles*, Renewable Energy, Vol. 80, pp. 724–736, Aug. 2015.

[14] **Koukoura, C., Natarajan, A.** and **Vesth, A.**, *Identification of support structure damping of a full scale offshore wind turbine in normal operation*, Renewable Energy, Vol. 81, pp. 882–895, 2015.

[15] **van Vondelen, A. A. W., Navalkar, S. T., Iliopoulos, A., van der Hoek, D. C.** and **van Wingerden, J.-W.**, *Damping identification of offshore wind turbines using operational modal analysis: a review*, Wind Energy Science, Vol. 7, pp. 161–184, 2022.

[16] **Norén-Cosgriff, K.** and **Kaynia, A. M.**, *Estimation of natural frequencies and damping using dynamic field data from an offshore wind turbine*, Marine Structures, Vol. 76, pp. 102915, Mar. 2021.

[17] **Bajric, A., Hogsberg, J.** and **Rudinger, F.**, *Evaluation of damping estimates by automated Operational Modal Analysis for offshore wind turbine tower vibrations*, 2017.

[18] **Christensen, S. S., Manzoni, S., Vanali, M., Cigada, A.** and **Brandt, A.**, *Quantitative Study on the Modal Parameters Estimated Using the PLSCF and the MITD Methods and an Automated Modal Analysis Algorithm*, pp. 159–168, Springer International Publishing, Oct. 2020.

[19] **Orlowitz, E.**, Damping estimation in operational modal analysis, Ph.D. thesis, University of Southern Denmark, 2015.

[20] **Orlowitz, E.** and **Brandt, A.**, *Influence of Noise in Correlation Function Estimates for Operational Modal Analysis*, *Topics in Modal Analysis & Testing, Volume 9*, pp. 55–64, Springer International Publishing, Jul. 2018.

[21] **Tarpø, M., Friis, T., Olsen, P., Juul, M., Georgakis, C.** and **Brincker, R.**, *Automated reduction of statistical errors in the estimated correlation function matrix for operational modal analysis*, Mechanical Systems and Signal Processing, Vol. 132, pp. 790–805, Oct. 2019.

[22] **Häckell, M. W.** and **Rolfes, R.**, *Monitoring of a 5 MW offshore wind energy converter – Condition parameters and triangulation-based extraction of modal parameters*, Mechanical Systems and Signal Processing, Vol. 40, No. 1, pp. 322–343, 2013.

[23] **Christensen, S. S.** and **Brandt, A.**, *Automatic operational modal analysis using statistical*

modelling of pole locations, *28th International Conference on Noise and Vibration Engineering*, pp. 2927–2938, 2018.

[24] **Christensen, S. S.** and **Brandt, A.**, *Time domain modal parameter estimation methods used in OMA: A comparison*, *8th International Operational Modal Analysis Conference, IOMAC 2019*, pp. 507–509, IOMAC, 2019.

[25] **Kjeld, J. G.** and **Brandt, A.**, *Pragmatic uncertainty bounds on modal parameters from an offshore wind turbine and its supporting structure*, *Proceeding of ISMA conference at Leuven, Belgium, September 2020*, 2020.

[26] **Avitabile, P.** and **Pingle, P.**, *Prediction of Full Field Dynamic Strain from Limited Sets of Measured Data*, Shock and Vibration, Vol. 19, No. 5, pp. 765–785, 2012.

[27] **Allemang, R. J.** and **Brown, D. L.**, *Experimental modal analysis and dynamic component synthesis. Volume 3: Modal parameter estimation*, Tech. rep., Cincinnati University Ohio, Department of Mechanical and Industrial Engineering, 1987.

[28] **Ibraham, S.**, *A method for the direct identification of vibration parameter from the free response*, Shock and Vibration Bulletin, Vol. 47, No. 4, 1977.

[29] **Overschee, P. V.** and **Moor, B. D.**, Subspace Identification for Linear Systems, Springer US, 1996.

[30] **Brandt, A.**, Noise and Vibration Analysis: Signal Analysis and Experimental Procedures, John Wiley & Sons Ltd., Jan. 2011.

[31] **Allemang, R. J.** and **Brown, D. L.**, *A correlation coefficient for modal vector analysis*, *Proc. 1st International Modal Analysis Conference, Orlando, FL*, 1982.

[32] **Hansen, M. H., Thomsen, K., Fuglsang, P.** and **Knudsen, T.**, *Two methods for estimating aeroelastic damping of operational wind turbine modes from experiments*, Wind Energy, Vol. 9, No. 1-2, pp. 179–191, Jan. 2006.

[33] **Chen, C.** and **Duffour, P.**, *Modelling damping sources in monopile-supported offshore wind turbines*, Wind Energy, Vol. 21, No. 11, pp. 1121–1140, Jun. 2018.